Land Imaging with Reconstructed High-Resolution Seasat-A Scatterometer Data: An Amazon Experiment

P.J. Hardin[1], D.G. Long[2]

Brigham Young University
690 H SWKT
Provo, Utah 84602

[1]Department of Geography, [2]Department of Electrical and Computer Engineering

ABSTRACT

Satellite wind scatterometers are microwave radars designed to measure near-surface wind speed and direction over the oceans. This was the primary mission for the Seasat-A Scatterometer (SASS), which acquired 14.6 Ghz data over 50 km resolution cells during its three month mission in 1978. However, an image reconstruction technique utilizing overlap in resolution cells from successive satellite orbits can improve that spatial resolution to 5 km over land. An experiment conducted on a reconstructed image of central South America illustrates the potential of this imagery for discriminating between tropical forest, woodland, and tropical grass-shrubland. The potential for deriving geophysical information from reconstructed scatterometer imagery of the earth's surface is discussed.

INTRODUCTION

Satellite scatterometers are active microwave radar instruments originally designed to measure the radar backscatter of the ocean's surface under all-weather conditions. Between June and October of 1978, the Seasat-A Satellite Scatterometer (SASS) was able to obtain nearly continuous global coverage at a spatial unit cell resolution of 50 km until a catastrophic short-circuit in the satellite's electrical system terminated subsequent data acquisition. Although Seasat-A operated for only 99 days, the wind vector information derived from SASS data conclusively showed accurate wind velocity measurements could be made from scatterometers on polar orbiting platforms. At the time of this writing, several additional spaceborne scatterometers are either currently active or in various planning stages.

The mission for SASS was acquisition of data for the determination of ocean surface wind direction and velocity. However, this paper will present results of an experiment designed to determine whether SASS imagery reconstructed to a 5 km resolution using a new technique[1] possesses adequate information for discriminating between broad vegetation formations of central South America.

HIGH RESOLUTION SCATTEROMETRY

Spaceborne scatterometers transmit microwave pulses to the ocean surface and measure backscattered power received at the instrument, allowing estimation of the normalized radar cross section (σ^o) of the surface. In simple terms, the radar cross section can be considered the target albedo at radar frequencies. From each illuminated location on the earth, the total power received by a radar is the sum of the power backscattered by the target, noise from the frequency-specific natural emissivity of the earth-atmosphere system, and noise from the instrument itself. Once noise is subtracted from the total received power, σ^o can then be calculated using the basic radar equation.

The observed σ^o of a given resolution element depends on 1) the target character such as roughness, conductivity, etc. and 2) the incidence angle and azimuth angle of the observation. When it can be assumed there is no azimuthal modulation of σ^o, a commonly accepted model for the incidence angle dependence of σ^o is

$$10\log_{10}\sigma^o(\theta) = \mathcal{A} + \mathcal{B}(\theta - 40°)$$

or alternatively

$$\sigma^o(\theta) = \alpha^{\mathcal{A}}[\beta(\theta)]^{\mathcal{B}}$$

where $\mathcal{A}$ and $\mathcal{B}$ are independent of the incidence angle θ and dependent on the target character, and where β is dependent on θ. It should be noted that $\mathcal{A}$ is the value of σ^o where θ equals 40°.

As described previously [1], the signal processing required for achieving higher resolution depends on overlap in the SASS σ^o measurements. However, the SASS σ^o measurements made by a single antenna on a single beam during one orbit have no overlap whatsoever, and the forward and aft beam measurements are overlapped only a small amount. Furthermore, when this lack of overlap is combined with the problem of small gaps in the surface coverage for a single orbit, the result is insufficient data to attempt the resolution improvement scheme with data from a single SASS pass. However, due to precession in the spacecraft orbit, a point on the earth's surface was observed from the same beam with slightly different azimuth and incidence angles about once every three days. Data was also acquired by the instrument on both ascending and descending orbital nodes. The resulting set of criss-crossing measurement swaths in a single orbit combined from several orbits provides ample overlap to create high resolution $\mathcal{A}$ and $\mathcal{B}$ images over much of the earth by utilizing a highly modified block algebraic reconstruction technique. The fidelity of the resulting high resolution imagery is dependent on several factors [1].

DISCRIMINATION METHODOLOGY

A simple experiment was devised to test the utility of the reconstructed imagery for discriminating between broad vegetation classes within the non-Andean portion of central South America (Figure 1). Using the 1:5,000,000 scale *Vegetation Map of South America* [2], large homogeneous rectangular regions for 18 different vegetation formations were delimited. Realizing the limitations of the map source material, the inexact nature of cartographic classification, unavoidable generalizations, and the difficulties in drawing exact boundaries for vegetation classes which likely blend in transition zones, the rectangular areas were delimited only for the larger map polygons of vegetation. The high resolution $\mathcal{A}$ and $\mathcal{B}$ images for the region were constructed, and pixel values were then extracted for each of the rectangular regions and saved for further analysis. Since the $\mathcal{B}$ image possessed very little discrimination power, only the high resolution $\mathcal{A}$ image is presented here (Figure 2). In the discrimination tests described below, only one half of the pixels for each of the 18 formations were used for training. The remaining half were reserved for testing the discrimination.

The fundamental procedural approach used in the supervised discriminant analysis was to continually regroup the original 18 categories into a much smaller set until the classification accuracy produced by quadratic discriminant functions reached an acceptable level. However, potential groupings which would require tenuous interpretations were not allowed. For example, the floristic formations designated as forest types on the UNESCO map were never mixed with members of the grassland category. Conversely, some of members in the woodland category might logically be grouped in the shrub category without insurmountable interpretation

91-72810/92$03.00 © IEEE 1992

problems.

In the ultimate discriminant analysis, the goal was to determine whether sufficient statistical distance in the A and B coefficient data existed between the final supervised land cover groupings for successful land cover mapping. Using the training set alone, quadratic discriminant functions were calculated for each of the final groups. These functions were then used to classify each pixel from the verification set. The agreement between each pixel's predicted and actual group was summarized in confusion matrix form for accuracy assessment. The quality of the supervised classification was assessed by calculating both an overall Cohen's kappa (κ) measure and a simple percentage.

FINDINGS AND DISCUSSION

Attempts to classify the original 18 categories without any regrouping produced a classification accuracy of only 57% (κ = 0.52). From the confusion matrix (Table 1) and graphical analysis it was clear substantial backscatter existed within groups considered forest, woodland, shrubland, and grassland. However, there was apparently good discrimination between these broad groups. Logically regrouping the 18 group data set to these four groups improved the classification accuracy to 81% (κ = 0.74). Combining the shrubland group with the grassland group to create a shrub-grassland category generated a marked improvement (94%, κ = 0.91). Table 2 summarizes the A and B information for each of the original 18 cover categories as subdivided into these three final categories. Table 3 presents the confusion matrix resulting from the experiment.

As mentioned previously, the first general group with the highest A coefficients was forest. It consisted of two moist tropical ombrophilous forest types, moist evergreen seasonal forest, tropical evergreen seasonal lowland forest, ombrophilous submontane forest, and associated degraded forest mosaics. The second general group consisted of four woodland vegetation formations, associated mosaics and degraded woodland landscapes. The specific woodland types included drought deciduous woodland known as *chaco*, thorn forest with succulents/*caatinga*, related degraded woodland formations/mosaics, and degraded *caatinga* formations. The grass-shrublands group consisted of several separate shrubland and grassland categories. These included two floristic formations of *campos cerrados, campos sujos/limpos*, grassland with palms, and seasonally flooded grassland or *pantanal*. Two varieties of degraded formations and cultivated crops were also members of this category.

The first confusion matrix (Table 1) indicates the greatest confusion problems between the forest and woodland groups to be primarily a result of backscatter overlap between degraded woodland formations and tropical evergreen seasonal lowland forest. The small amount of confusion remaining exists primarily between the woodland and grass-shrubland group. While there is some backscatter resemblance between most members of the woodland and grass-shrubland groups, the two degraded woodland formations appear to be major culprits in several instances. This confusion reflects the common remote sensing task of distinguishing between woodland and shrublands when both are so heterogeneous with variable canopy densities, species compositions, plant spacing, tree heights, and canopy response to seasonal factors. For example, there is substantial confusion between the degraded woodland formation (with crops) and the shrubby grassland *campos sujos*. It is highly likely that a woodland degraded through cattle grazing, fire, and agriculture would exhibit a great variance of backscatter dependent on the areal extent of the degradation, its severity, or the successional stage of any sub-climax regrowth. Thus it is entirely reasonable that some regions of degraded woodland would exhibit similar backscatter characteristics to the shrubby grassland of *campos sujos* or the pure grassland of *campos limpos*.

SUMMARY

When classified using supervised methods, it appears reconstructed SASS imagery had potential for discriminating between tropical forest, tropical woodlands, and tropical grass-shrublands. Forest was almost perfectly divisible from woodland and grass-shrubland, while there remained some (albeit minor) backscatter similarity between some members of the woodland and grass-shrubland groups. In every instance, degradation of a vegetation formation resulted in decreased backscatter. While pure agricultural land was indistinguishable from grass and shrubland, it was entirely divisible from humid forest and subhumid woodland. The consistency of the classification results, particularly the degraded formations, seems to indicate the different backscatter groups were manifestations of differences in canopy densities. We also suspect some of the confusion may be due to different communities being at different stages of seasonal vigor. The likelihood of both these possibilities is high, given that the study area covered one half of a continent with strong seasonal precipitation changes in several savanna regions containing a variety of vegetation formations.

FINAL COMMENTS

Given the success of this discrimination experiment, further research into subtropical land scatterometry may bring substantial payoffs. While the goal of this project was not to create a 1978 vegetation map of central South America, it may be possible to do such mapping with SASS data. In such a project, much of the confusion in the purely backscatter-based classification could be removed by incorporating topographic, climatic, and other ancillary data sources. It may be possible to extend the procedure using the global SASS data set to all the subtropical regions of the world in order to estimate and map the 1978 extent of the global subtropical forests into broad categories. With the launch of ADEOS in 1995 and the high resolution ground processing of NSCAT imagery using similar techniques, the potential may exist to to assess change in the subtropical forest character and extent over the seventeen year interval at identical spatial resolutions and frequencies. Unlike the SASS data which covered only three months, NSCAT coverage of the equatorial and savanna regions for the entire year would also allow change in backscatter through the seasons to be used as a discriminator for more accurate vegetation mapping. It would also allow real-time monitoring of global subtropical seasonal changes without interference from cloud cover which afflicts visible and near-infrared instruments.

However, the potential for utilizing reconstructed SASS (or other scatterometer) imagery goes beyond land cover mapping or monitoring. The existence of several vegetation class gradations within and between the formations indicates the strong possibility of obtaining critical quantitative information about subtropical vegetation community character from reconstructed scatterometer imagery. While these results lead us to believe that 14.6 Ghz backscatter in subtropical areas is a function of canopy density, it is possible these backscatter coefficients also change in response to canopy vigor, canopy moisture, another canopy structural characteristic, or more complex quantitative variables.

Land scatterometry can potentially play an important role in tropical studies requiring fusion of data from sensors of different spatial resolutions. Using higher resolution SAR, visible, thermal, and infrared imagery of carefully selected field sites as primary data sources, it may be possible to use high resolution reconstructed scatterometer imagery to extend derived estimates of biomass, canopy structure, moisture content, or transpiration rates over large regions.

The SASS image reconstruction technique also holds great promise for land imaging of other regions of interest during the late summer months of 1978. These include the world's boreal forests, Greenland,

and the Antarctic. The potential for imaging glacial and sea ice is particularly fascinating, since scatterometer images provide multiple incidence angle observations. It may be possible to create several coregistered high-resolution images, each possessing a different range of incidence angles, to infer ice age, water content, snow cover, or other parameters of interest.

Given the potential for scatterometers to obtain useful information over land, it may be profitable for the scientific community to carefully consider both NSCAT and its follow-on EoS-era scatterometers as sources for land imaging. According to recent research, minor modifications involving changes to the digital subsystem combined with ground signal processing algorithms could produce reconstructed image resolutions between 1 and 3 km [1]. These changes would make NSCAT and the EoS-era scatterometers dual mission instruments which could provide ground imaging at 14 Ghz with a spatial resolution compatible with several other EoS instruments including the Multifrequency Imaging Microwave Radiometer (MIMR), Multi-angle Imaging Spectro-Radiometer (MISR), and the Moderate Resolution Imaging Spectrometer (MODIS).

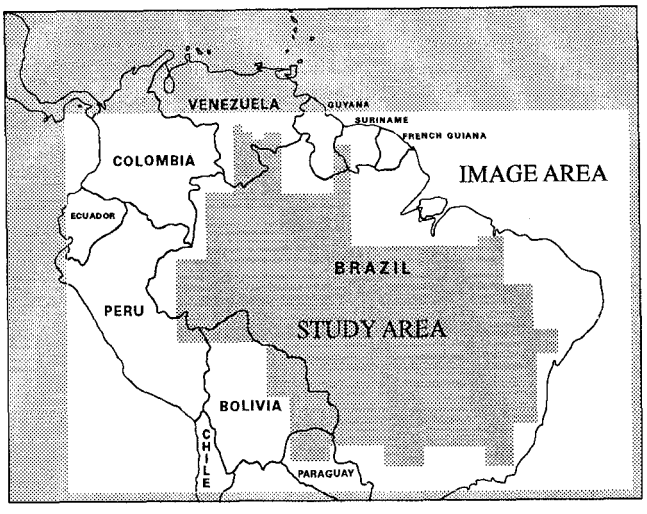

Figure 1. The study area

REFERENCES

[1] Long, D.G., P.J. Hardin, and P.T. Whiting, 1992. High Resolution Imaging of Land/Ice using Spaceborne Scatterometry Part I: The Imaging Technique. Submitted to *IEEE Transactions on Geoscience and Remote Sensing.*

[2] UNESCO, 1980. *Vegetation Map of South America.* 1:5,000,000, two sheets. Published by the United Nations Educational, Scientific and Cultural Organization, Paris.

Figure 2. The reconstructed $\mathcal{A}$ image

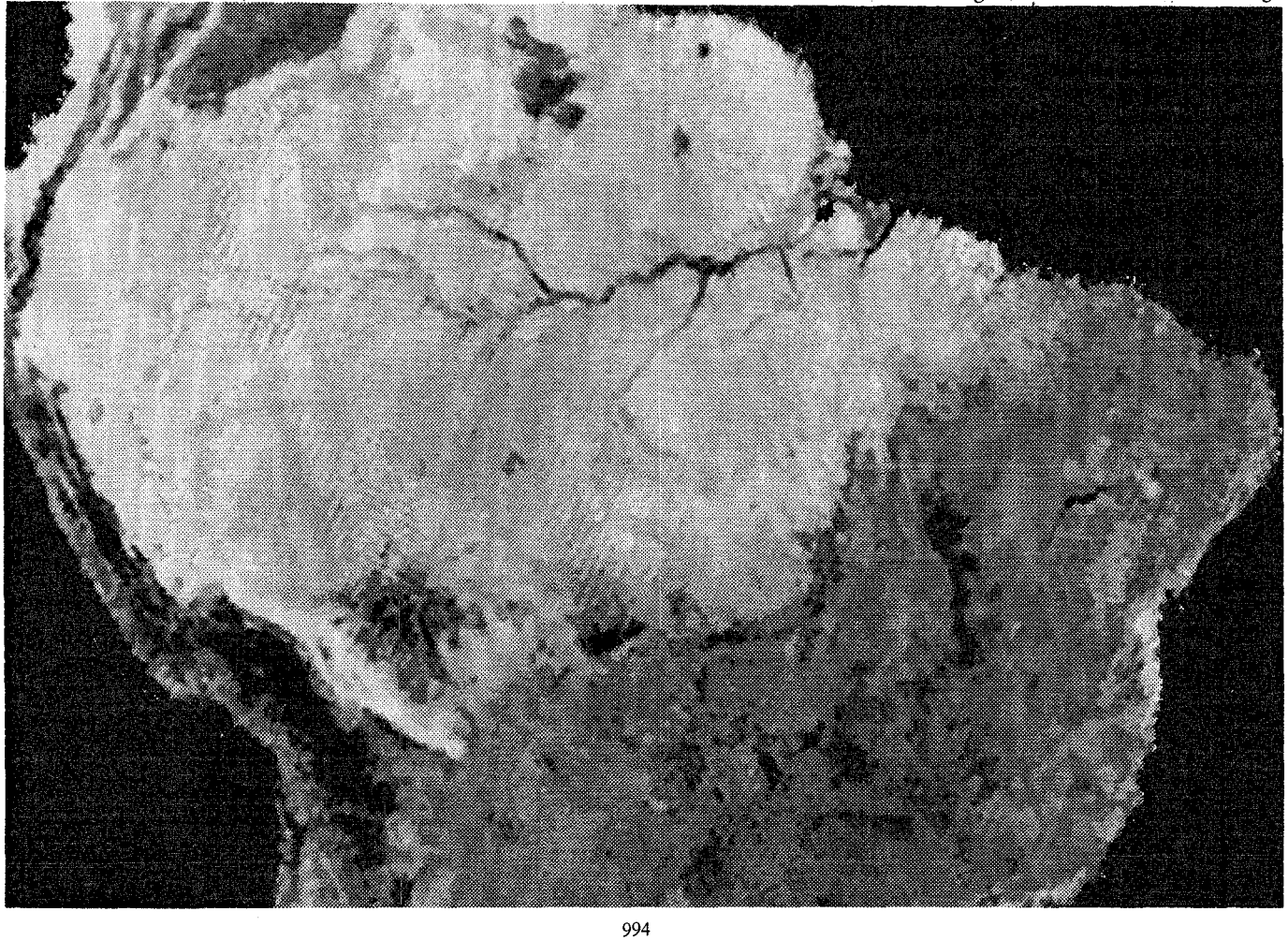

		Actual Class																	
		Forest						Woodland				Grass-Shrubland							
	Predicted Class	1	2	3	4	5	6	7	8	9	10	11	12	13	14	15	16	17	18
Forest	1	126	149	89	34	41	73	0	0	0	0	0	0	0	98	0	0	0	0
	2	90	1120	52	719	62	110	2	0	0	0	0	0	0	54	7	0	0	0
	3	5	0	92	14	0	0	0	0	0	0	0	0	0	0	0	0	0	0
	4	11	767	17	4149	0	5	14	0	0	0	0	0	0	3	0	0	0	0
	5	6	35	4	0	8	14	1	0	0	0	0	0	0	13	4	3	0	0
	6	0	22	4	35	0	33	17	0	17	0	0	0	0	3	0	6	0	0
Woodland	7	0	7	9	16	8	27	398	0	89	19	79	0	0	96	29	63	68	4
	8	0	0	0	9	0	3	0	2507	116	2	0	0	0	0	0	0	0	12
	9	0	0	0	2	0	35	5	58	335	14	11	0	0	0	0	41	0	1
	10	0	0	0	0	0	0	0	21	194	103	92	0	30	8	0	12	0	72
Grass-Shrubland	11	0	0	17	0	3	0	43	0	133	28	1220	7	92	96	34	473	372	227
	12	0	0	0	0	0	0	0	0	0	0	18	280	0	171	85	17	158	88
	13	0	0	0	0	0	0	0	0	0	0	30	0	40	4	7	62	12	77
	14	0	0	0	0	0	0	20	0	31	0	0	7	0	174	20	46	21	141
	15	0	0	0	0	0	0	0	0	2	0	0	0	0	13	1	0	0	11
	16	0	0	0	0	0	0	0	0	0	0	28	0	41	2	29	42	65	36
	17	0	0	8	0	0	0	0	0	13	0	301	48	27	123	85	83	346	138
	18	0	0	0	0	0	0	0	6	3	2	182	0	104	157	21	210	230	211

Table 1. Confusion matrix from classifying the 18 vegetation formations without any regrouping.

	Vegetation Formation	Class n	Mean $\mathcal{A}$	Stdv. $\mathcal{A}$	Mean $\mathcal{B}$	Stdv. $\mathcal{B}$
Forest	Extremely moist forest (1)	238	-7.19	0.193	-0.124	0.002
	Moist seasonal forest (2)	2100	-7.54	0.203	-0.122	0.003
	Ombrophilous submontane forest (3)	293	-7.50	1.006	-0.121	0.002
	Very moist forest (4)	4978	-7.67	0.203	-0.118	0.002
	Degraded forest formations (5)	121	-7.54	0.400	-0.125	0.004
	Tropical evergreen seasonal lowland forest (6)	300	-7.84	0.589	-0.123	0.003
Woodland	Degraded woodland formations (7)	499	-8.59	0.373	-0.124	0.002
	Chaco (8)	2592	-9.46	0.494	-0.106	0.003
	Caatinga (9)	933	-9.30	0.696	-0.118	0.007
	Degraded caatinga woodland formations (10)	168	-9.82	0.472	-0.116	0.003
Grass - Shrubland	Campos cerrados N (11)	1961	-10.04	0.681	-0.122	0.004
	Degraded subhumid campos cerrados and crops (12)	342	-11.18	0.491	-0.131	0.002
	Degraded lowland campos cerrados (13)	334	-10.65	0.563	0.119	0.002
	Campos sujos and limpos (14)	1015	-10.14	1.641	-0.127	0.004
	Grassland with palms (15)	321	-10.77	1.126	-0.127	0.003
	Pantanal (16)	1058	-10.33	0.938	-0.122	0.002
	Cultivated crops (17)	1273	-10.43	0.903	-0.125	0.003
	Campos cerrados S (18)	918	-10.94	0.734	-0.121	0.004

Table 2. Summary training statistics for the 18 original groups.

	Actual Class		
Predicted Class	Forest	Woodland	Grass-Shrubland
Forest	7892	88	217
	98%	2%	3%
Woodland	110	3763	377
	1%	90%	5%
Grass-Shrubland	28	342	6628
	.3%	8%	92%
Total	8030	4193	7222
	100%	*100%*	*100%*

Table 3. Final confusion matrix for the 3 group discrimination.